

# Calculating the Structural Responses of Aquaculture Tanks by Considering the Effects of Corrosion and Tank Sloshing

Zhiyong Sun<sup>1</sup>, Hui Li<sup>1</sup>, Siqi Zhou<sup>2</sup>, Zhiyu Li<sup>3</sup> and Guoqing Feng<sup>1</sup>

Received: 15 February 2023 / Accepted: 18 April 2023

© Harbin Engineering University and Springer-Verlag GmbH Germany, part of Springer Nature 2024

## Abstract

The environment and structure of the tanks used in aquaculture vessels are remarkably different from those of ordinary ships, and the resulting problem of structural strength is related to breeding safety. In this study, a model of aquaculture tank corrosion was constructed by using the multiphysical field coupling analysis software COMSOL Multiphysics, and wave and sloshing loads were calculated on the basis of potential flow theory and computational fluid dynamics. The influence of different calculation methods for corrosion allowance and sloshing load on the structural responses of aquaculture tanks was analyzed. Through our calculations, we found that the corrosion of aquaculture tanks is different from that of ordinary ships. The corrosion allowance in *Rules for the Classification of Sea-going Steel Ships* is small, and the influence of the aquaculture environment on corrosion can be ignored. Compared with the method set in the relevant rules, our proposed coupling direct calculation method for the structural response calculation of aquaculture tanks can better combine the specific environment of aquaculture tanks and provide more accurate calculations.

**Keywords** Aquaculture tank; Corrosion simulation; Sloshing load; Design load; Structural response

## 1 Introduction

Aquaculture vessels, a new type of aquaculture equipment for deep-sea fishery, can provide a suitable environment for the breeding of fish in tanks at sea (Guo et al., 2020; Xue et al., 2022). Given the particular function of aquaculture tanks, the seawater they contain can severely corrode their bulkhead to jeopardize their structural safety. The sloshing load of aquaculture water in tanks caused by hull motion also has a great influence on their structural safety (Cui et al., 2022; Hui et al., 2022).

Although numerous studies have investigated the effects of sloshing load on structural strength, most focused on ships carrying liquid cargo, such as oil tankers and LNG carriers (Dumitrache and Deleanu, 2020; Park et al., 2021). The empirical formula for calculating the strength of tank structures in the presence of a sloshing load has been proposed by the classification societies of various countries. Among the proposed methods, the simplest involves calculating the sloshing load on the basis of an empirical formula and using it to evaluate structural strength (Zhang, 2018). Current studies in the effects of sloshing load on structural strength focus on direct and effective numerical methods. For example, Park et al. (2023) investigated the dynamic responses of an LNG cargo containment system by using the triangular impulse response function. Yun et al. (2020) developed two-way cosimulation technology on the basis of DualSPHysics and RecurDyn and applied it to solve the problem of sloshing inside a tank connected to the upper plate of a six-DOF platform. They investigated the effects of the dynamic load of fluid on structural safety. Lee and Paik (2021) examined nonlinear impact structural response characteristics under sloshing impact loads by utilizing a nonlinear finite element ANSYS/LS-DYNA method. Dumitrache and Deleanu (2020) studied the influence of tank sloshing caused by hull motion on the strength of ballast tank structures and found that the cyclic mechanical stress caused by sloshing can produce fatigue stresses in the welded joints

## Article Highlights

- The aquaculture tank corrosion was constructed by using the multiphysical field coupling analysis.
- CFD-based tank sloshing load of aquaculture tanks was performed.
- The structural responses of aquaculture tanks by considering the effects of corrosion and tank sloshing were calculated, showing that the method proposed in this paper is accurate.

✉ Hui Li  
huili@hrbeu.edu.cn

<sup>1</sup> College of Shipbuilding Engineering, Harbin Engineering University, Harbin 150001, China

<sup>2</sup> Guangdong Institute of Intelligent Unmanned System, Guangzhou 511458, China

<sup>3</sup> Marine Design & Research Institute of China, Shanghai 200011, China

of hulls. Hwang and Lee (2021) extended the velocity of sloshing flow (calculated by CFD) to the real scale and applied it in a local two-way fluid–structure interaction analysis of the load conditions and structural response of LNGs.

Although numerous simplified corrosion models have been proposed to study hull corrosion in a specific environment or specific steel, these models have certain limitations (Ivošević et al., 2017; Zayed et al., 2018; Yao et al., 2018). COMSOL Multiphysics software has emerged as a potential tool for analyzing corrosion and variation in different parameters. For example, Iwamoto (2019) conducted validation by comparing corrosion simulation results from COMSOL Multiphysics and experimental results obtained by using the mock-up sheet pile model. They verified that the potential distributions obtained from experimental results were consistent with those acquired through simulations. Gupta et al. (2022) investigated the galvanic corrosion behavior of rivet-joint systems by using time-dependent simulation with the help of COMSOL Multiphysics software. In addition, Prajapati et al. (2022), Chalgham et al. (2019), and Feng et al. (2022) conducted corrosion simulation calculations by using COSMOL Multiphysics software and achieved satisfactory results.

In some special environments, corrosion has a great effect on the strength of ship structures. Vu and Dong (2020) introduced a probabilistic model to estimate the rate of corrosion and assessed the effects of corrosion in flanges and webs on the cross-sectional properties and ultimate strength of bulk carriers. Georgiadis and Samuelides (2019) reassessed ultimate strength by updating the time-variant corrosion model and exploiting on-site observations from thickness measurement reports within the framework of Bayesian updates. Given that aquaculture vessels are a new type of deep-sea aquaculture equipment, their working environment and structural form are considerably different from those of ordinary vessels. No relevant structural rules are currently available for the strength assessment of aquaculture vessels. In addition, the conventional method for calculating corrosion allowance in strength assessment involves using the empirical values recommended by classification societies. However, during operation, the proportion of the area of contact between seawater or aquaculture water and the inner or outer surfaces of ships is large. In addition to the conventional components of seawater, aquaculture water contains substances that may cause marine steel to corrode. These substances include feed, fungicides, nutrients, and fish excrement. Various factors indicate that the problem of corrosion in aquaculture vessels is more serious than that in ordinary vessels (Feng et al., 2022). Therefore, the corrosion allowance recommended in the rules for ordinary vessels may be unsuitable for aquaculture vessels.

In this study, the working characteristics of aquaculture vessels were considered, and a model for analyzing the structure of aquaculture tanks was established. The corro-

sion simulation of aquaculture tanks based on multiphysical field coupling analysis was proposed by considering the working environment of aquaculture vessels. Wave and sloshing loads were calculated on the basis of potential flow theory and computational fluid dynamics (CFD), respectively. Furthermore, the influence of corrosion allowance and sloshing load calculated by different calculation methods on aquaculture structural responses was analyzed. Finally, a coupling direct calculation method for the structural responses of aquaculture tanks was proposed and used to calculate structural responses.

## 2 Calculation model

The aquaculture vessel used in this study is equipped with 16 aquaculture tanks in two rows along the ship, as shown in Figure 1. The internal structure of the tanks is depicted in Figure 2. The vessel conducts aquaculture operations in the Yellow Sea and East China Sea. The main dimensions of the vessel and tank are given in Table 1.



**Figure 1** Aquaculture vessel

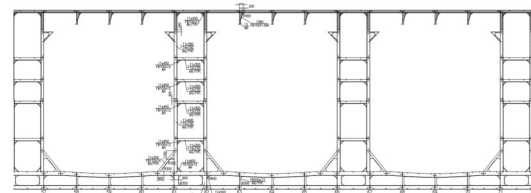


**Figure 2** Structural layout of aquaculture tanks

**Table 1** Main dimensions of the aquaculture vessel and tank

Parameter	Parameter value
Overall length (m)	258.2
Length between perpendiculars (m)	250.6
Breadth (m)	44.0
Depth (m)	22.8
Draft (m)	14.0
Displacement (t)	136 734.0
Longitudinal center of gravity (m)	125.79
Vertical center of gravity (m)	11.81
Radius of roll gyration (m)	15.4
Radius of pitch gyration (m)	58.0
Radius of yaw gyration (m)	58.7
Tank length (m)	17.8
Tank breadth (m)	19.0
Tank water level height (m)	16.8

### 3 Multiphysical field coupled simulation calculation of corrosion

#### 3.1 Basic principle

##### 3.1.1 Electrode reaction

Corrosion is a special redox reaction. During the corrosion of aquaculture tanks, steel is in contact with seawater. Given that water molecules are polar, they strongly attract the iron ions that are in direct contact with seawater. The relevant chemical reaction is as follows:

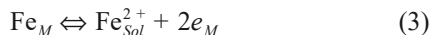


where Fe is the iron atom,  $Fe^{2+}$  is the ferrous ion,  $M$  is the solid phase, and Sol is the liquid phase.

The concentration of ferrous ions in the water increases with the progression of corrosion. Ferrous ions accumulate near the interfacial region to form a high concentration gradient, which in turn causes them to react to form iron atoms attached to the metal phase. The chemical reaction is as follows:



The reactions represented by the above two equations occur simultaneously in corrosion as follows:



Gibbs' free energy is the basis for judging whether the corrosion reaction can proceed. Whether the redox reaction can occur spontaneously can be determined in accordance with the following formula:

$$\Delta G = v_C \mu_C + v_D \mu_D - (-v_A \mu_A - v_B \mu_B) \tag{4}$$

where  $\Delta G$  is the change in Gibbs' free energy,  $A$  and  $B$  are reactants,  $C$  and  $D$  are products of the reaction,  $v$  is the stoichiometric number of the substance, and  $\mu$  is its electrochemical potential.

When  $\Delta G < 0$ , the reaction can occur spontaneously.

When  $\Delta G > 0$ , the reaction cannot occur spontaneously.

When  $\Delta G = 0$ , the reaction reaches a state of chemical equilibrium, and the reaction rates in the forward and reverse directions are equal.

When the reaction has been determined to be capable of occurring spontaneously during corrosion, whether the reaction proceeds in the forward or reverse direction at a certain point in time must also be determined. The product of the stoichiometric number and chemical potential during the reaction is divided by the product of the charge in the reactive ion and Faraday constant, which is called the Galvani potential and is represented by  $\varphi$ :

$$\varphi = \frac{\sum_j v_j \mu_j}{nF} \tag{5}$$

When a redox reaction reaches equilibrium, the Galvani potential calculated in accordance with the above formula is called the equilibrium potential of the reaction and is represented by  $\varphi_e$ .

When  $\varphi_e > \varphi$ , the reaction proceeds in the positive direction.

When  $\varphi_e < \varphi$ , the reaction proceeds in the negative direction.

When  $\varphi_e = \varphi$ , the reaction reaches a state of dynamic equilibrium.

##### 3.1.2 Corrosion mathematical model

In corrosion simulation, corrosion needs to satisfy the mass transfer conservation, charge conservation, and local electric neutrality equations, as shown in Equations (6), (7), and (8), respectively:

$$\frac{\partial c_i}{\partial t} + \nabla N_i = 0 \tag{6}$$

where  $c$  is substance concentration,  $i$  is the type of substance, and  $t$  is the time item. The flux  $N$  is calculated as

$$N_i = -D \nabla c_i - z_i u_{m,i} F c_i \nabla \varphi_l + c_i u, \tag{7}$$

where  $-D \nabla c_i$  is the diffusion term,  $u_m$  is the electromigration number,  $z_i u_{m,i} F c_i \nabla \varphi_l$  is the electric migration item, and  $c_i u$  is the convective term.

The net current in the electrolyte is described by using the total material flux

$$i_l = F \sum z_i N_i \tag{8}$$

The charge conservation and local electric neutrality equations are

$$\nabla i_l = Q_l \tag{9}$$

$$\sum z_i c_i = 0 \tag{10}$$

#### 3.2 Corrosion model

We believe that the corrosion of aquaculture tanks is a coupling problem of multiple physical fields. In accordance with the theory of corrosion electrochemistry, corrosion often occurs at sharp points, corners, or weld seams wherein surface geometry is severely discontinuous, given the presence of strong electrolytes in seawater. These locations exhibit particularly severe corrosion due to their high corrosion current density. However, as corrosion occurs, the morphology of these positions gradually changes, and sharp positions may be passivated, leading to a decrease in corrosion current density and a change in structural corrosion characteristics. From the perspective of the overall structure,

a high density of corrosion current is generated at the new location. This situation indicates that the corrosion location has changed. In addition, in actual corrosion simulation analysis, the vertical gradient change of oxygen concentration should be considered, and oxygen concentration is another important factor affecting corrosion. The corrosion of aquaculture tanks can be seen as a coupling problem of multiple physical fields. Such a problem should at least include the coupling of solid structure, distribution of corrosion electrochemical parameters, and distribution of physical parameters (such as oxygen concentration).

Corrosion in different regions of aquaculture tanks differs. In accordance with the characteristics of the seawater environment of aquaculture tanks, corrosion regions can be divided into splash, main, and sediment corrosion regions (Figure 3). A real-scale finite element model was established in accordance with the size of the aquaculture tank in the multiphysics coupling analysis software COMSOL Multiphysics (Figure 4). The structures near the waterline, hatch corners, and weld seams are refined on the basis of the coarse grid.

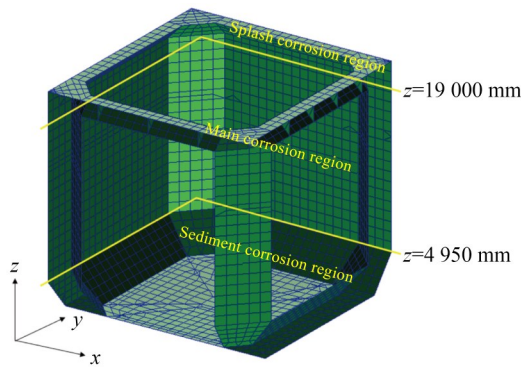


Figure 3 Corrosion regions in an aquaculture tank

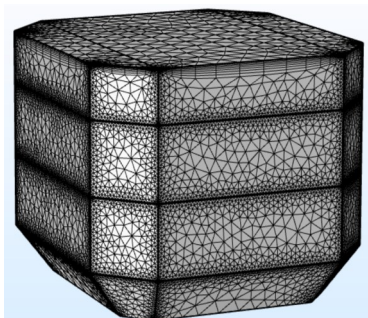


Figure 4 Finite element model of an aquaculture tank in COMSOL

### 3.3 Hydrological conditions of aquaculture tanks

The hydrological condition and electrochemical parameters of aquaculture tanks are key parameters affecting the results of corrosion simulation. The parameters of the hydrological conditions and electrochemical parameters in accor-

dance with the species of fish being bred in the aquaculture vessel are shown in Tables 2 and 3.

Table 2 Hydrological conditions of aquaculture water

Parameters	Normal range	Harmful threshold
Dissolved oxygen, O <sub>2</sub> (mg/l)	6–9	<5
Nitrogen, N <sub>2</sub> (%)	80–100	>100
Carbon dioxide, CO <sub>2</sub> (mg/l)	10–20	>20
Ammonia, NH <sub>3</sub> /NH <sub>4</sub> -N (mg/l)	0–5	>5
Nitrite, NO <sub>2</sub> -N (mg/l)	0–1.5	>1.5
Nitrate, NO <sub>3</sub> -N (mg/l)	50–100	>90
Alkalinity, CaCO <sub>3</sub> (mg/l)	100–250	<50
pH	6.5–8.5	<6, >8.5
Water temperature (°C)	12–15	>18
Suspended particulates (mg/l)	0–10	–

Table 3 Electrochemical parameters of aquaculture water

Parameters	Parameters value
Equilibrium potential of welding flux (V)	–0.58
Exchange current density of welding flux (A/m <sup>2</sup> )	0.001
Tafel slope of flux electrode (mV)	–160
Equilibrium potential of iron (V)	1.55
Exchange current density of iron (A/m <sup>2</sup> )	0.10
Tafel slope of iron electrode (mV)	50
Ultimate current density of iron (A/m <sup>2</sup> )	100
Conductivity of aquaculture water (S/m)	2.5
Molar mass of iron (kg/mol)	0.056

### 3.4 Calculations in corrosion simulation

The lifecycle of aquaculture vessels is 20 years. Corrosion simulations were conducted for the 20-year lifecycle of the vessel studied in this work. COMSOL Multiphysics analysis commercial software was used to simulate tank corrosion in accordance with the relevant theory of the electrochemistry of corrosion and in consideration of the hydrological conditions of the aquaculture tank and corresponding anticorrosion measurement (epoxy paint as an anticorrosive coating). The corrosion thicknesses of the tank structures for 20 years were calculated. The results are shown in Figures 5 and 6.

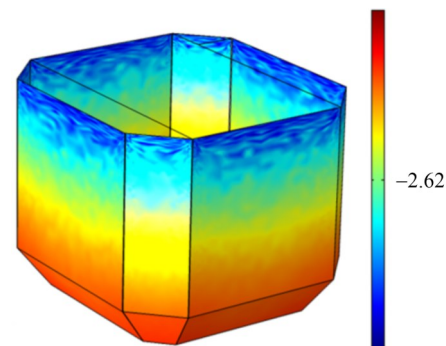
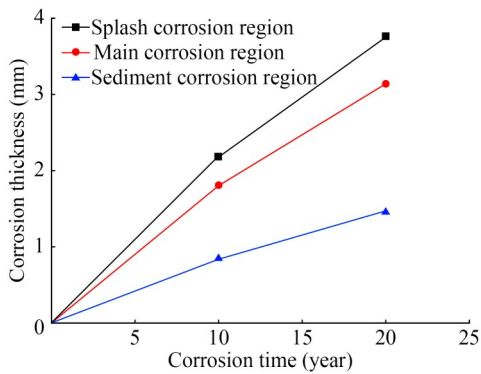


Figure 5 Cloud image of corrosion thickness in the aquaculture tank



**Figure 6** Simulation of corrosion thickness in aquaculture tanks

Figure 5 is the cloud image of the corrosion thickness of the aquaculture tank. The most severe corrosion occurs in the bulkhead near the waterline, that is, in the splash corrosion region. Figure 6 shows that over the 20-year period, the maximum corrosion thickness in the splash corrosion region is 3.79 mm. The structures in this region are near the liquid surface, which is humid all year round. The air around the structures contains a large amount of chloride, which exerts a strong decomposing effect on the oxide film on the surface of the aquaculture tank, aggravating the effect of corrosion and causing the most serious corrosion in this region. Corrosion in the sediment corrosion region over 20 years is relatively small, with a maximum thickness of 1.46 mm. Among the regions, the sediment corrosion region is the farthest from the water surface. Seawater has a low oxygen concentration. Therefore, galvanic corrosion mainly occurs in this region. The welding materials used at the weld of the plate are different from the materials of the hull plate. They are in direct contact with each other, creating conditions for the occurrence of galvanic corrosion. The corrosion thickness of the structure in the main corrosion region is between those in the splash and sediment corrosion regions. In this region, the maximum thickness is 3.16 mm over 20 years. The structure of the main corrosion region is located below the waterline and is completely immersed in seawater. Seawater acts as a good conductor of ions to create conditions for corrosion. At the same time, because this region contains abundant oxygen, corrosion occurs in this region. However, given that the oxygen content in the water in the main corrosion region is not as high as that in the splash corrosion region, the degree of corrosion in this region is smaller than that in the splash corrosion region. The cloud image of the corrosion thickness in the main corrosion region illustrates that with the increase in depth, corrosion thickness gradually decreases because the concentration of oxygen in seawater varies with depth.

The structure of aquaculture vessels is similar to that of double-hulled oil tankers. Currently, the strength assessment of the aquaculture tank is usually conducted by referring to the relevant classification society’s rules for double-hulled oil tankers, such as the China Classification Society’s

(CCS) Rules for the Classification of Sea-going Steel Ships (Han et al. 2020). The comparison between the corrosion allowance specified in CCS rules and the simulation results of corrosion is shown in Table 4 (provisions for corrosion allowance are specified in Part 9, Chapter 3, Section 1 in Rules for the Classification of Sea-going Steel Ships).

**Table 4** Comparison of corrosion allowance unit: mm

Tank region	Simulated corrosion value	Value in rules
Splash corrosion region	3.79	1.70
Main corrosion region	3.16	1.40
Sediment corrosion region	1.46	1.40

The provisions for the corrosion allowance of oil tankers in CCS rules are based on empirical values. Given that the environment in aquaculture tanks is more corrosive than that in oil tanks, the simulated results of 20 years are larger than the corrosion allowances given in CCS rules. The literature states that the average corrosion rate of a steel structure in seawater is 0.11–0.14 mm/year and that the local corrosion rate can reach as high as 0.6 mm/year (Lan et al. 2012). In the simulation of corrosion over 20 years, the average thickness of corrosion in the aquaculture tank was 2.80 mm, and the average corrosion rate was 0.139 mm/year, which is consistent with the measurement results in the references. We also compared the measured corrosion rates of 441 KW (600 PS) steel fishing vessels built by the Dalian Ocean Fisheries Group Shipyard in Liaoning Province, China (Qu et al. 1988). These fishing vessels operate in the East China Sea and the Yellow Sea, consistent with the working status and environment of the aquaculture vessel studied in this work. The average corrosion rate of the steel fishing vessel fish tank is 0.143 mm/year, which is close to the simulation result of 0.139 mm/year. Therefore, simulating the corrosion of an aquaculture water tank through multiphysical field coupling analysis is correct.

## 4 Calculation of design loads

### 4.1 Wave load

#### 4.1.1 Mathematical model

In accordance with three-dimensional linear potential flow theory, the total velocity potential in flow fields is

$$\phi(x, y, z, t) = [ -Ux + \phi_s(x, y, z) ] + \text{Re} \{ \phi_T(x, y, z) e^{i\omega t} \} \tag{11}$$

where  $-Ux$  is the uniform flow,  $\phi_s(x, y, z)$  is the wave-making potential, and  $\phi_T(x, y, z) e^{i\omega t}$  represents the unsteady velocity potential of waves. The unsteady velocity potential can be

decomposed into the following form:

$$\phi_T(x, y, z) = \phi_I(x, y, z) + \phi_D(x, y, z) + \phi_R(x, y, z) \quad (12)$$

where  $\phi_I(x, y, z)$  is the incidence potential,  $\phi_D(x, y, z)$  is the diffraction potential, and  $\phi_R(x, y, z)$  represents the radiation potential.

In accordance with the theory of rigid body dynamics, the motion equation of ships in regular waves can be expressed as

$$[M]\{\ddot{\eta}(t)\} = \{F(t)\} = \{F\}e^{i\omega t} \quad (13)$$

where  $\{F(t)\} = \{F^S(t)\} + \{F^D(t)\}$ .

$\{F^S(t)\}$  represents the hydrostatic load, which can be expressed as

$$\{F^S(t)\} = \iint_S P_S(x, y, z, t)\{n\}ds = -[C]\{\eta(t)\} \quad (14)$$

where  $P_S(x, y, z, t)$  is the hydrostatic pressure caused by ship motion, and  $[C]$  is the hydrostatic coefficient.

$\{F^D(t)\}$  is the hydrodynamic load, which can be expressed as

$$\{F^D(t)\} = \{F_I(t)\} + \{F_D(t)\} + \{F_R(t)\} \quad (15)$$

where  $\{F_I(t)\}$ ,  $\{F_D(t)\}$ , and  $\{F_R(t)\}$  represent the incident, diffraction, and radiation wave forces, respectively. On the basis of plane wave theory and the Bernoulli equation, the pressure distribution is obtained by deriving the incident, diffraction, and radiation potentials. The pressure distribution on the wet surface of the ship is integrated to obtain incident, radiation and diffraction forces. The expressions for incident, radiation and diffraction forces are

$$\{F_I(t)\} = \iint_S p_I(x, y, z)\{n\}ds \cdot e^{i\omega t} \quad (16)$$

$$\{F_D(t)\} = \iint_S p_D(x, y, z)\{n\}ds \cdot e^{i\omega t} \quad (17)$$

$$\{F_R(t)\} = \iint_S p_R(x, y, z)\{n\}ds \cdot e^{i\omega t} \quad (18)$$

$$\begin{aligned} \{F^D(t)\} &= \{F_I(t)\} + \{F_D(t)\} + \{F_R(t)\} \\ &= -i\omega\rho \sum_{j=1}^6 \eta_j \cdot \left[ \iint_S \left( i\omega - U \frac{\partial}{\partial x} \right) \cdot \phi_j(x, y, z)\{n\}ds \right] \cdot e^{i\omega t} \\ &= -[A]\{\ddot{\eta}(t)\} - [B]\{\dot{\eta}(t)\} \end{aligned} \quad (19)$$

Subsequently, the linear frequency domain rigid body dynamics equation for ship motion in regular waves is

$$\begin{aligned} ([M] + [A])\{\ddot{\eta}(t)\} + [B]\{\dot{\eta}(t)\} \\ + [C]\{\eta(t)\} = \{f(t)\} = \{f\}e^{i\omega t} \end{aligned} \quad (20)$$

where  $[M]$  is the hull mass matrix;  $[A]$  is the additional mass matrix of the hull;  $\{\eta(t)\}$  represents the hull motion with six degrees of freedom;  $[B]$  is the fluid damping coefficient;  $[C]$  is the hydrostatic coefficient;  $\{f(t)\}$  is the wave interference force; and  $\{f\}e^{i\omega t}$  is the form after the spatio-temporal separation of wave interference forces.

#### 4.1.2 Design wave method

The loads for structural analysis were calculated by using the design wave method. The design wave expression is

$$f(t) = A \cdot \cos(\omega t + \varepsilon_m + \varepsilon) \quad (21)$$

where  $A$  is the amplitude of the design wave;  $\omega$  is the frequency;  $\varepsilon_m$  is the phase corresponding to the maximum value of the load transfer function; and the sum of  $\varepsilon_m$  and  $\varepsilon$  is equal to  $0^\circ$  or  $180^\circ$ , which correspond to the sagging and hogging states, respectively.

The wave direction and frequency corresponding to the maximum value of the response amplitude operators of the main control load are the design wave direction and frequency. The design wave amplitude is calculated by using

$$A = \frac{\text{design value of main control load}}{\text{maximum value of response amplitude operators}} \quad (22)$$

where the design value of the main control load is calculated through long-term analysis.

#### 4.1.3 Wave load calculation

The wave loads of the aquaculture vessel were calculated by using the commercial software COMPASS-WALCS-Basic on the basis of 3-D potential flow theory. The stats of the East China Sea and Yellow Sea, wherein the aquaculture vessel operates, were used in the calculation of the design loads. The exceeding probability was determined in accordance with the number of waves encountered during a 20-year service period. Given that the sloshing load is an important load acting on the tank structures, it was selected as the main control load in addition to the vertical bending moment. Tank sloshing is mainly excited by the roll motion of the vessel. Therefore, roll motion was used as the main control load instead of sloshing load in design load calculation.

By using parameterized modeling methods, the hull surface mesh is divided on the basis of hull shape lines. The hydrodynamic mesh of the hull surface is shown in Figure 7 (a). The floating state is adjusted in accordance with the mass distribution of the hull, and the obtained wet surface mesh and calculation sections are shown in Figure 7 (b).

Then, the long-term prediction of wave loads was conducted, and the long-term prediction values of the main control loads are listed in Table 6. The parameters of the design waves are shown in Table 7.

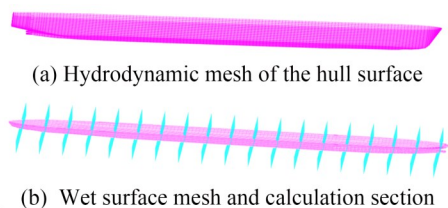
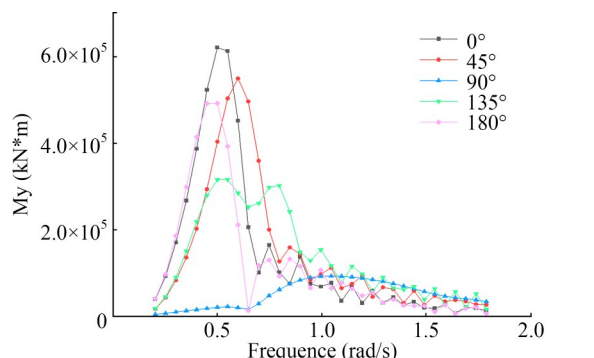


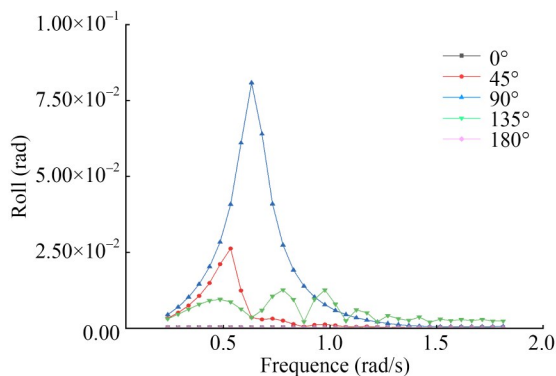
**Figure 7** Hydrodynamic calculation model

**Table 5** Parameters of wave load calculation

Calculation parameter	Parameter value
Wave direction (°)	0, 45, 90, 135, 180
Wave frequency (rad/s)	0.2, 0.4, 0.6, 0.8, 1.0, 1.1, 1.2, 1.3, 1.4, 1.5, 1.6, 1.7, 1.8, 1.9, 2.0
Exceeding probability	1.27E-8



(a) Transfer function of the vertical bending moment of section



(b) Transfer function of roll motion

**Figure 8** Amplitude frequency response results

**Table 6** Values of the vertical bending moment and roll response and long-term prediction values.

Main control parameter	Long-term value	Response value
My (kN·m)	3.69E+6	6.22E+5
Roll (rad)	2.76E-1	8.15E-2

**Table 7** Parameters of the design wave

Load condition	Main control loads	Value	Wave heading	Wave amplitude (m)	Frequency (rad/s)	Phase (°)
LC01-1	Wave load	Maximum	Head wave	5.94	0.5	325.9
LC01-2	Wave load	Minimum	Head wave	5.94	0.5	145.9
LC02-1	Sloshing load	Maximum	Beam wave	3.39	0.6	162.1
LC02-2	Sloshing load	Minimum	Beam wave	3.39	0.6	342.1

## 4.2 Calculation of sloshing loads

### 4.2.1 Mathematical model

The incompressible viscous flows of two immiscible fluids, i.e., air and water, are governed by Reynolds-averaged Navier–Stokes equations (Equations (1) and (2)).

$$\frac{\partial \rho}{\partial t} + \nabla \cdot (\rho \bar{\mathbf{v}}) = 0 \tag{23}$$

$$\frac{\partial}{\partial t} (\rho \bar{\mathbf{v}}) + \nabla \cdot (\rho \bar{\mathbf{v}} \otimes \bar{\mathbf{v}}) = -\nabla \cdot \bar{p} \mathbf{I} + \nabla \cdot (\bar{\mathbf{T}} + \mathbf{T}_{\text{RANS}}) + \mathbf{f}_b \tag{24}$$

where  $\rho$  is the fluid density,  $\rho = 1\,024 \text{ kg/m}^3$ ;  $\bar{\mathbf{v}}$  is the mean velocity;  $\bar{p}$  is the mean pressure;  $\mathbf{I}$  is the identity tensor;  $\bar{\mathbf{T}}$  is the mean viscous stress tensor; and  $\mathbf{f}_b$  is the resultant of the body forces. The additional term ( $\mathbf{T}_{\text{RANS}}$ ) is the stress tensor, which has the following definition:

$$\mathbf{T}_{\text{RANS}} = -\rho \left( \begin{array}{ccc} \overline{u'u'} & \overline{u'v'} & \overline{u'w'} \\ \overline{u'v'} & \overline{v'v'} & \overline{v'w'} \\ \overline{u'w'} & \overline{v'w'} & \overline{w'w'} \end{array} \right) + \frac{2}{3} \rho k \mathbf{I} \tag{25}$$

where  $k$  is the turbulent kinetic energy.

We use the standard  $k - \epsilon$  SST model to simulate turbulent flow. The transport equations for kinetic energy  $k$  and specific dissipation rate  $\omega$  are

$$\frac{\partial}{\partial t} (\rho k) + \nabla \cdot (\rho k \bar{\mathbf{v}}) = \nabla \cdot [(\mu + \sigma_k \mu_t) \nabla k] + P_k - \rho \beta^* f_{\beta^*} (\omega k - \omega_0 k_0) \tag{26}$$

$$\frac{\partial}{\partial t} (\rho \omega) + \nabla \cdot (\rho \omega \bar{\mathbf{v}}) = \nabla \cdot [(\mu + \sigma_\omega \mu_t) \nabla \omega] + P_\omega - \rho \beta f_\beta (\omega^2 - \omega_0^2) \tag{27}$$

where  $\mu$  is the turbulent kinetic energy;  $\sigma_k$  and  $\sigma_\omega$  are the model coefficients,  $\sigma_k = 0.5$  and  $\sigma_\omega = 0.5$ ; and  $P_k$  and  $P_\omega$  are production terms.  $f_{\beta^*} = 1$ ;  $f_\beta$  is the vortex-stretching modification factor,  $f_\beta = 1$ ;  $k_0$  and  $\omega_0$  are the ambient turbulence values that counteract turbulence decay.

### 4.2.2 Calculation of sloshing loads

The tank sloshing load was calculated by using the CFD software STAR-CCM+. Pitch motion was considered in the structural analysis because it can also induce sloshing in aquaculture tanks under head sea conditions. High sloshing

**Table 8** Calculation of structural responses under working conditions

Working condition	Wave loads	Calculation method	
		Corrosion allowance	Sloshing loads
WC01-1	LC01-1	By Rules	By Rules
WC01-2	LC01-2	By Rules	By Rules
WC02-1	LC02-1	By Rules	By Rules
WC02-2	LC02-2	By Rules	By Rules
WC03-1	LC01-1	Multiphysical field coupling analysis	By Rules
WC03-2	LC01-2	Multiphysical field coupling analysis	By Rules
WC04-1	LC02-1	Multiphysical field coupling analysis	By Rules
WC04-2	LC02-2	Multiphysical field coupling analysis	By Rules
WC05-1	LC01-1	By Rules	CFD
WC05-2	LC01-2	By Rules	CFD
WC06-1	LC02-1	By Rules	CFD
WC06-2	LC02-2	By Rules	CFD
WC07-1	LC01-1	Multiphysical field coupling analysis	CFD
WC07-2	LC01-2	Multiphysical field coupling analysis	CFD
WC08-1	LC02-1	Multiphysical field coupling analysis	CFD
WC08-2	LC02-2	Multiphysical field coupling analysis	CFD

amplitudes can be expected when the frequency of tank motion is close to the natural frequency of a fluid. For a given rectangular prismatic tank, the natural frequencies of the fluid, depending on the fill depth, are given by

$$\omega_n^2 = g \frac{n\pi}{L} \tanh\left(\frac{n\pi}{L} d\right) \quad (28)$$

where  $L$  is the tank width,  $d$  is the water depth, and  $n$  is the mode number. In accordance with Equation (28), the natural frequency of the tank is 1.31 rad/s. The natural frequency of ship roll motion is 0.6 rad/s. Given that the motion response of the ship is very small at 1.31 rad/s, the tank response caused by ship motion will not occur. Therefore, the calculation in this study ignores tank resonance.

Roll and pitch motions were regarded as the external excitation of the sloshing in the tank, and the expression of the motions in the numerical simulation is

$$X(t) = A \sin \omega t \quad (29)$$

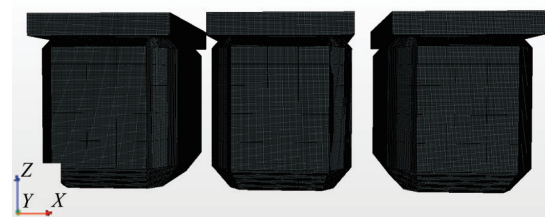
where  $A$  and  $\omega$  are the amplitude and frequency of external excitation, respectively.

On the basis of the design wave parameters in Table 7, the amplitudes of the pitch and roll motions were calculated by using COMPASS-WALCS-Basic. Subsequently, the results, as shown in Table 9, were input into the numerical simulation of tank sloshing.

**Table 9** Parameters of the external excitation of tank sloshing

Working condition	Motion	Amplitude $A$ (rad)	Frequency $\omega$ (rad/s)
WC05-1, WC05-2 WC07-1, WC07-2	Pitch	6.359E-2	0.5
WC06-1, WC06-2 WC08-1, WC08-2	Roll	2.760E-1	0.6

The CAD software CATIA V5 was used to generate the geometric model of the aquaculture tank. The geometric model was then imported into STAR-CCM+. The top of the tank was set as a pressure outlet boundary, and the rest of the walls were set with wall boundary conditions. The standard  $k - \varepsilon$  SST model was used to simulate turbulent flow. Grid convergence analysis was performed, and the size of grids used for calculation was determined to be 0.1 m (see Figure 9). The cloud image of the sloshing pressure calculated at  $1/4 T_1$  under WC06-1 is shown in Figure 10 (a), and the time history curve of sloshing dynamic pressure is provided in Figure 10 (b). ( $T_1$  is the period of the roll motion under the WC06-1 working condition).

**Figure 9** STAR-CCM+ computational grid model

Sloshing pressure was calculated in accordance with the provisions for sloshing pressure in Part 9, Chapter 4, Section 6 in *Rules for the Classification of Sea-going Steel Ships* to compare the CFD and CCS rule methods. Comparison results are shown in Table 10. The dynamic pressure calculated on the basis of CCS rules is greater than the dynamic pressure calculated on the basis of CFD.

## 5 Structural response calculation

### 5.1 Finite element calculation model

Part 9, Chapter 7, Section 2 in *Rules for the Classification of Sea-going Steel Ships* stipulates the selection range of calculation cabins. Therefore, tanks No. 5–10 were selected

as targets in the structural response calculation. The finite element model in Patran is shown in Figure 11.

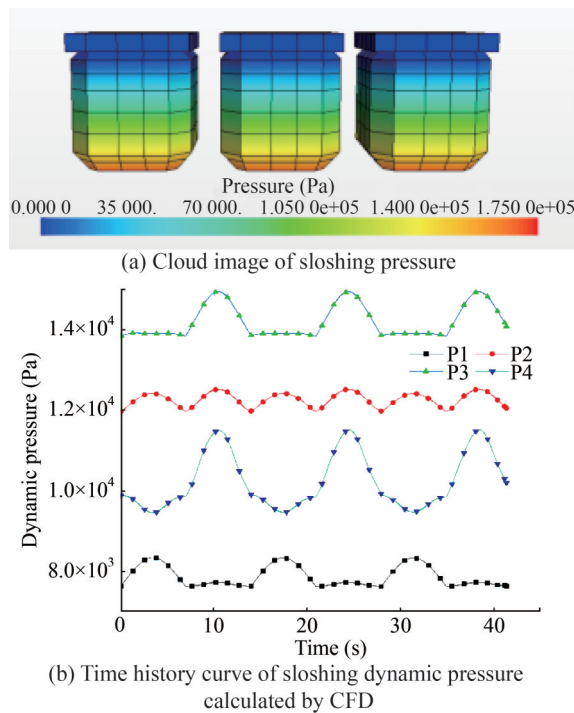


**Figure 10** Cloud image and time history curve of sloshing pressure

**Table 10** Comparison of sloshing loads

Number	Position (m)	Dynamic pressure (Pa)	
		Rules	CFD
P1	(125.8, -18.6, 3.1)	12 726	7 890
P2	(125.8, -20.0, 6.2)	17 070	12 266
P3	(125.8, -20.0, 12.8)	17 073	14 208
P4	(125.8, -20.0, 18.0)	16 875	10 258

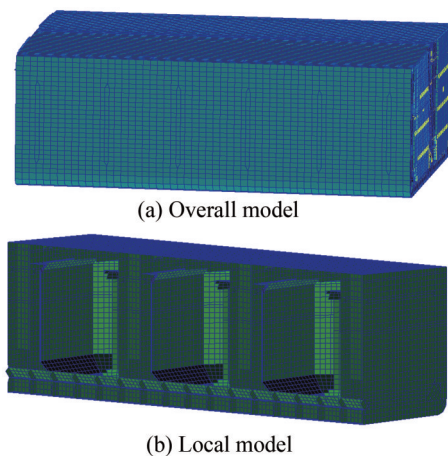


**Figure 11** Finite element model of the aquaculture tank

## 5.2 Results and discussion

The commercial FEA software Patran/Nastran was used to calculate the structural response of the tank model. The

direct calculation loads in Section 4.1. are used for wave loads in all calculation conditions. The calculation working conditions are shown in Table 8. In the analysis of results, the tank structures were divided into several typical parts, such as the bottom plate, bottom inclined plate, transverse bulkhead, and longitudinal bulkhead.

### 5.2.1 Effect of corrosion allowance

The corrosion allowance in WC01-1, WC01-2, WC02-1, and WC02-2 were calculated in accordance with CCS rules. The calculation results for structural stress are shown in Table 11. The corrosion allowance in W03-1, WC03-2, WC04-1, and WC04-2 was calculated by the multiphysical field coupling analysis described in Section 3, and the calculation results of structural stress are shown in Table 12. Comparing the stress under the same wave loads and sloshing load working conditions revealed that the stresses of the bottom plate under WC03-1 and WC03-2 are 4.8% and 4.5% larger than those under WC01-1 and WC01-2, respectively. Similarly, the stresses of the bottom inclined plate under WC03-1 and WC03-2 are 0.9% and 0.7% larger than those under WC01-1 and WC01-2, respectively. The structural stresses calculated on the basis of the simulated corrosion allowance are similar to those calculated on the basis of the corrosion allowance stipulated in CCS rules because the bottom plate and bottom inclined plate are located in the sediment corrosion region, and the corrosion simulation calculation value of this part is close to the value stated in CCS rules. The stresses of the transverse bulkhead under WC04-1 and WC04-2 are 17.4% and 18.0% larger than those under WC02-1 and WC02-2, respectively. The stresses of the longitudinal bulkhead under WC04-1 and WC04-2 are 11.7% and 11.0% larger than those under WC02-1 and WC02-2, respectively. The results of structural stress calculated by using two kinds of corrosion allowances differ greatly at the transverse and longitudinal bulkheads because the corrosion allowance of transverse and longitudinal bulkheads in the splash and the main corrosion regions calculated through simulation is quite different from the values in CCS rules. In view of the overall structure, the structural stress calculated by the corrosion simulation value is approximately 8% larger than the corrosion value in the rules.

**Table 11** Stress calculation results of tank structures based on rules  
Unit: MPa

Tank structure	WC01-1	WC01-2	WC02-1	WC02-2
Bottom inclined plate	114.0	143.0	133.0	135.0
Bottom plate	105.0	133.0	122.0	133.0
Transverse bulkhead	71.1	90.1	86.9	91.5
Longitudinal bulkhead	90.6	109.0	103.0	109.0

### 5.2.2 Effect of sloshing load

The sloshing loads in WC05-1, WC05-2, WC06-1, and WC06-2 were calculated by using the CFD method intro-

**Table 12** Stress calculation results of tank structure based on corrosion simulation Unit: MPa

Tank structure	WC03-1	WC03-2	WC04-1	WC04-2
Bottom inclined plate	115.0	144.0	134.0	136.0
Bottom plate	110.0	139.0	127.0	139.0
Transverse bulkhead	81.9	106.0	102.0	108.0
Longitudinal bulkhead	101.0	121.0	115.0	121.0

**Table 13** Stress calculation results of tank structure based on sloshing load calculated by CFD method Unit: MPa

Tank structure	WC05-1	WC05-2	WC06-1	WC06-2
Bottom inclined plate	92.8	111.0	124.0	128.0
Bottom plate	62.7	76.9	76.1	139.0
Transverse bulkhead	56.3	61.5	67.1	75.0
Longitudinal bulkhead	63.0	88.2	82.0	88.7

duced in Section 4.2 and imported into Patran/Nastran by using the Patran Command Language interface for structural response calculation. The calculation results for structural stress are shown in Table 13. Comparing the stress under the same wave loads and corrosion allowance working conditions revealed that the stress of the bottom inclined plate under WC05-1 and WC05-2 are 18.6% and 22.0% smaller than those under WC01-1 and WC01-2, respectively. Similarly, the stress of the bottom plate under WC06-1 and WC06-2 are 37.6% and 37.4% smaller than those under WC02-1 and WC02-2, respectively. The structural stress of the sloshing load calculated by CFD is smaller than that calculated in accordance with CCS rules because, as discussed in Section 4.2, the sloshing load calculated by CFD is less than that calculated by the empirical formula given by CCS rules.

5.2.3 Effect of coupling direct calculation

Coupling direct calculation was applied to calculate structural responses in this study. In this method, corrosion allowance was calculated by the multiphysical coupling field method, and the sloshing load was calculated by the

CFD method. The process of coupling direct calculation is illustrated in Figure 12. The calculation results are shown in Table 14. Comparison with the structural stress results calculated on the basis of CCS rules in Table 11 shows that the stresses of the bottom inclined plate under WC07-1 and WC07-2 are 18.9% and 19.6% smaller than those under WC01-1 and WC01-2, respectively. The stresses of the bottom plate under WC08-1 and WC08-2 are 33.8% and 33.2% smaller than those under WC02-1 and WC02-2, respectively. Structural stress based on the coupling direct calculation method is significantly smaller than that based on the conventional method. In other words, if the conventional method is used to calculate the structural response of the aquaculture tank and the structural response results are used to check the structural strength, then the check results may be too conservative. This situation may easily lead to structural redundancy. Therefore, compared with the conventional method, the proposed coupling direct calculation method for the structural response calculation of aquaculture tanks can better combine the specific environment of aquaculture tanks and provide more accurate calculation results.

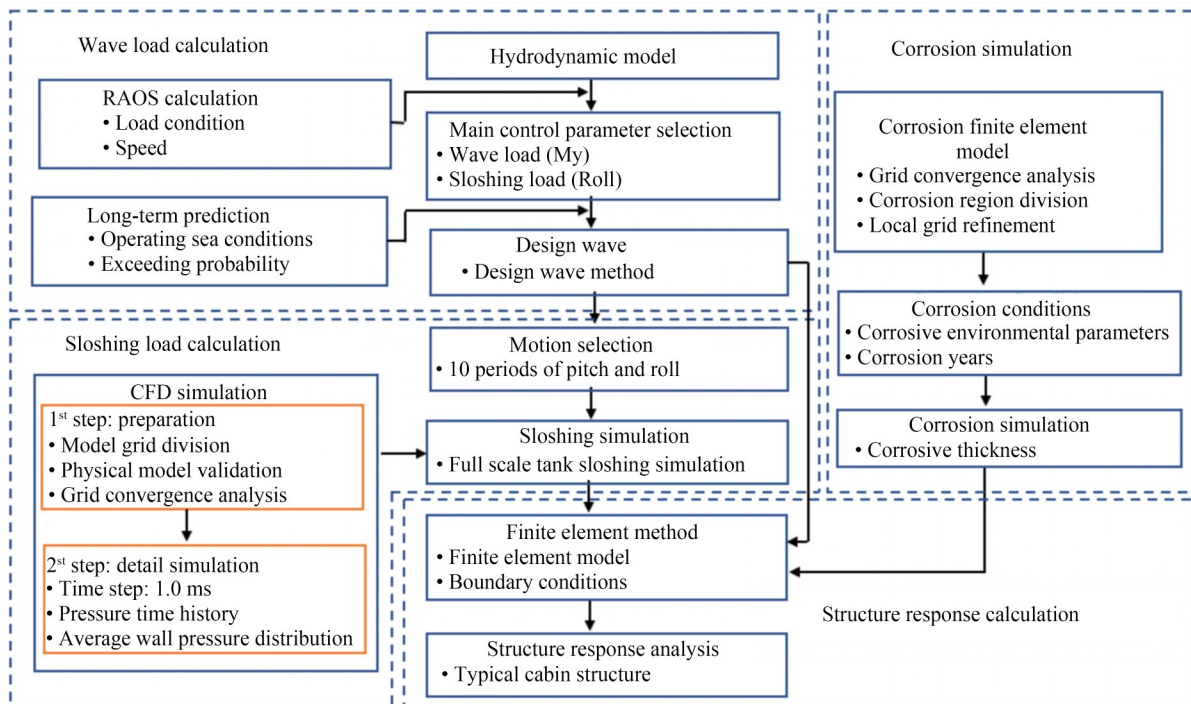


**Figure 12** Coupling direct calculation

**Table 14** Stress calculation results of tank structure based on coupling direct calculation Unit: MPa

Tank structure	WC07-1	WC07-2	WC08-1	WC08-2
Bottom inclined plate	92.5	115.0	125.0	130.0
Bottom plate	68.1	76.9	80.8	88.8
Transverse bulkhead	57.8	62.9	79.0	88.1
Longitudinal bulkhead	68.1	99.6	90.0	101.0

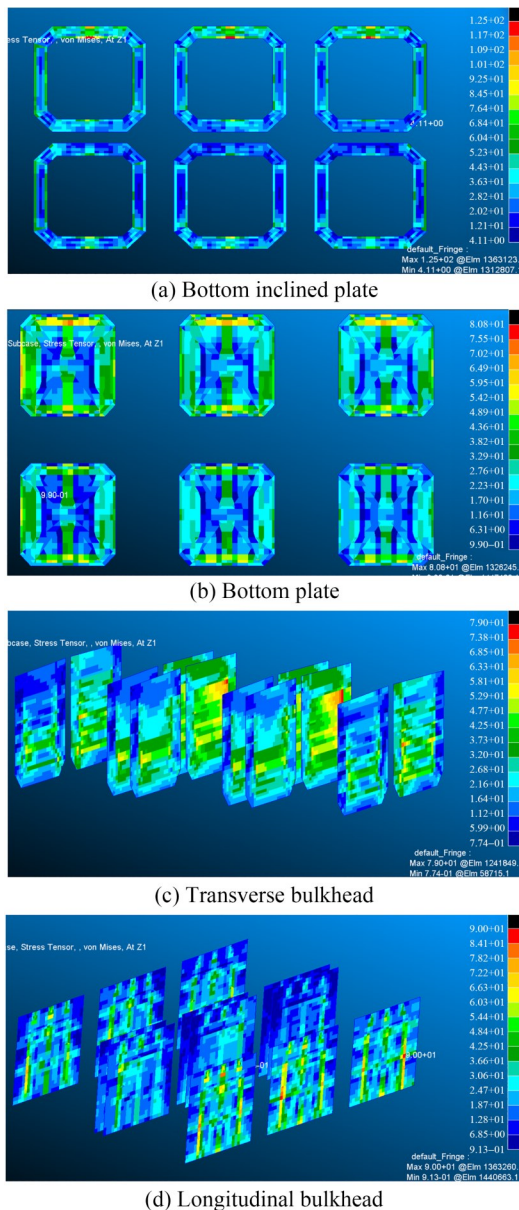


**Figure 13** Cloud image of structural stress in the sagging state under the working condition LC04

At the same time, compared with the structural stress calculation results under different main control loads in Table 14, the structural stress calculated on the basis of sloshing load is significantly larger than that calculated on the basis of wave load. The stresses of the bottom inclined plate under WC08-1 and WC08-2 are 26.0% and 11.5%

larger than those under WC07-1 and WC07-2, respectively. The stresses of the bottom plate under WC08-1 and WC08-2 are 15.7% and 13.4% larger than those under WC07-1 and WC07-2, respectively. We can conclude that due to the special sloshing environment and tank structure of aquaculture vessels, the sloshing load should be considered when determining the main control load for strength checks.

## 6 Conclusions

The corrosion of a 100 000-ton aquaculture vessel in the aquaculture environment was simulated through multiphysical field coupling analysis. The wave and sloshing loads on the aquaculture vessel were calculated on the basis of potential flow theory and the CFD method, respectively. The design load was determined on the basis of different main control parameters. The influence of different calculation methods for corrosion allowance and sloshing loads on aquaculture structural stress was analyzed. Finally, a coupling direct calculation method for the structural response of aquaculture tanks was proposed, and the structural response was calculated. The main conclusions are as follows:

- (1) The corrosion characteristics of aquaculture tanks are considerably different from those of ordinary ships, given their special aquaculture environment. The corrosion calculated through multiphysical field coupling analysis is closer to measurements than that calculated by using the traditional empirical formula.
- (2) Sloshing load has an important effect on the structure of aquaculture tanks. In the determination of the design load, the working condition under which the sloshing load is the main control parameter should be considered in addition to the wave load, which is considered the main control parameter in conventional practice.
- (3) The proposed coupling direct calculation method for the structural response calculation of aquaculture tanks can well combine the specific environment of aquaculture tanks and provide highly accurate calculation results.

**Funding** This work is financially supported by the National Natural Science Foundation of China (Grant No. 52071110) and Fundamental Research Funds for the Central Universities (Grant No. 3072022QBZ0101).

**Competing interest** The authors have no competing interests to declare that are relevant to the content of this article.

## References

Chalgham W, Wu KY, Mosleh A (2019) External corrosion modeling for an underground natural gas pipeline using COMSOL Multiphysics  
 Cui M, Li Z, Zhang C, Guo X (2022) Statistical investigation into

- the flow field of closed aquaculture tanks aboard a platform under periodic oscillation. *Ocean Eng* 248: 110677. <https://doi.org/10.1016/j.oceaneng.2022.110677>
- Dumitrache CL, Deleanu D (2020) Sloshing effect, fluid structure interaction analysis. *IOP Conf Ser Mater Sci Eng* 916: 012030. <https://doi.org/10.1088/1757-899X/916/1/012030>
- Feng GQ, Zhou SQ, Li Zhiyu, Li Yang (2022) Simulation analysis on corrosion of water tank structure of aquaculture ship. *Journal of Huazhong University of Science and Technology (Natural Science Edition)*: 1-8. <https://doi.org/10.13245/j.hust.230197>
- Georgiadis D, Samuelides M (2019) A methodology for the reassessment of hull-girder ultimate strength of a VLCC tanker based on corrosion model updating. *Ships Offshore Struct* 14: 270–280. <https://doi.org/10.1080/17445302.2019.1577599>
- Guo X, Li Z, Cui M, Wang B (2020) Numerical investigation on flow characteristics of water in the fish tank on a force-rolling aquaculture platform. *Ocean Eng* 217: 107936. <https://doi.org/10.1016/j.oceaneng.2020.107936>
- Gupta D, Kumar Y, Prajapati V, Kalam A, Dubey M (2022) Time dependent analysis of galvanic corrosion on mild steel with magnesium alloy (AE44) rivet-plate joint system using COMSOL Multiphysics Simulation. *J Bio- Tribo-Corros* 8: 111. <https://doi.org/10.1007/s40735-022-00710-z>
- Han B, Chen ZX, Cui MC, Wang QW, Wang YF (2020) Stability design criteria and checking methods of deep-sea aquaculture platform. *Ship Engineering*, 42(S2): 30-35. <https://doi.org/10.13788/j.cnki.cbgc.2020.S2.006>
- Hui L, Zhiyong S, Bingbing H, Yuhang S, Baoli D (2022) Research on the motion response of aquaculture ship and tank sloshing under rolling resonance. *Brodogradnja* 73: 1-15. <https://doi.org/10.21278/brod73201>
- Hwang S-Y, Lee J-H (2021) The numerical investigation of structural strength assessment of LNG CCS by sloshing impacts based on multiphase fluid model. *Appl Sci* 11: 7414. <https://doi.org/10.3390/app11167414>
- Ivošević Š, Meštrović R, Kovač N (2017) An approach to the probabilistic corrosion rate estimation model for inner bottom plates of bulk carriers. *Brodogradnja* 68: 57-70. <https://doi.org/10.21278/brod68404>
- Iwamoto T (2019) Validation as construction design method of anti-corrosion process for marine steel structures using COMSOL Multiphysics® through mock-up sheet piles
- Lan Z, Wang X, Hou B, Wang Z, Song J, Chen S (2012) Simulation of sacrificial anode protection for steel platform using boundary element method. *Eng Anal Bound Elem* 36: 903-906. <https://doi.org/10.1016/j.enganabound.2011.07.018>
- Lee SE, Paik JK (2021) Pressure-impulse diagram of The FLNG tanks under sloshing loads. *Int J Marit Eng* 160. <https://doi.org/10.5750/ijme.v160iA2.1051>
- Park YI, Lee SH, Kim J-H (2023) Study of applicability of triangular impulse response function for ultimate strength of LNG cargo containment systems under sloshing impact loads. *Appl Sci* 13: 2883. <https://doi.org/10.3390/app13052883>
- Park Y-J, Kim S, Cho J-R, Doh D-H, Cho G-R (2021) Fatigue life and effect of sloshing according to the scale ratio of a prismatic LNG tank. *J Mech Sci Technol* 35: 507-514. <https://doi.org/10.1007/s12206-021-0109-z>
- Prajapati V, Kumar Y, Gupta D, Kalam A, Dubey M (2022) Analysis of pitting corrosion of pipelines in a marine corrosive environment using COMSOL Multiphysics. *J Bio- Tribo-Corros* 8: 21. <https://doi.org/10.1007/s40735-021-00620-6>
- Qu GS, P ZW, Z GQ (1988) Research on corrosion of steel fishing vessels. *Journal of Dalian Fisheries College*. 53-62. <https://doi.org/10.16535/j.cnki.dlhyxb.1988.02.008>
- Vu VT, Dong DT (2020) Hull girder ultimate strength assessment considering local corrosion. *J Mar Sci Appl* 19: 693-704. <https://doi.org/10.1007/s11804-020-00169-9>
- Xue B, Zhao Y, Bi C, Cheng Y, Ren X, Liu Y (2022) Investigation of flow field and pollutant particle distribution in the aquaculture tank for fish farming based on computational fluid dynamics. *Comput Electron Agric* 200: 107243. <https://doi.org/10.1016/j.compag.2022.107243>
- Yao Y, Yang Y, He Z, Wang Y (2018) Experimental study on generalized constitutive model of hull structural plate with multi-parameter pitting corrosion. *Ocean Eng* 170: 407-415. <https://doi.org/10.1016/j.oceaneng.2018.10.038>
- Yun S-M, Kim S-P, Chung S-M, Shin W-J, Cho D-S, Park J-C (2020) Structural Safety Assessment of Connection between Sloshing Tank and 6-DOF Platform Using Co-Simulation of Fluid and Multi-Flexible-Body Dynamics. *Water* 12: 2108. <https://doi.org/10.3390/w12082108>
- Zayed A, Garbatov Y, Guedes Soares C (2018) Corrosion degradation of ship hull steel plates accounting for local environmental conditions. *Ocean Eng* 163: 299-306. <https://doi.org/10.1016/j.oceaneng.2018.05.047>
- Zhang MJ (2018) Strength assessment of independent type B LNG tank under sloshing loads and skeleton optimization. Master's thesis, Shanghai Jiao Tong University